

A new antenna array architecture with hybrid beamforming for broadband satellite communications

1st Margaux Pellet

Thales Alenia Space & Heriot-Watt
University

Toulouse, France

margaux.pellet@thalesaleniaspace.com

2nd George Goussetis

Heriot-Watt University
Edinburgh, UK

G.Goussetis@hw.ac.uk

3rd Hervé Legay

Thales Alenia Space
Toulouse, France

herve.legay@thalesaleniaspace.com

4th Joao Mota

Heriot-Watt University

Edinburgh, UK

J.Mota@hw.ac.uk

5th Bingen Cortazar

European Space Agency

Noordwijk, Netherlands

Bingen.Cortazar@esa.int

6th Giovanni Toso

European Space Agency

Noordwijk, Netherlands

Giovanni.Toso@esa.int

Abstract—In this paper, an antenna array architecture for broadband space communications with overlapped square subarrays is proposed. Analog and digital beamforming are performed consecutively at subarray level and across all subarrays. Subarrays are considered at digital beamforming level as large radiating elements, and thus the spacing between adjacent subarrays is not sufficient to prevent from interference. This leads to the creation of grating lobes. Overlapping methodologies have been studied in the literature and is an effective solution to mitigate this non-desired grating lobes. An overlapping strategy is proposed in this paper and can be seen as a shift by half the size of a subarray along 2-D. This enables a total mitigation of odd grating lobes. A comparison is made to benchmark this architecture performance compared to other existing strategies.

Keywords—analog beamforming, digital beamforming, subarrays, hybrid beamforming, overlap, grating lobes, scanning range, multi-beam antenna

I. INTRODUCTION

The transition from broadcast to broadband calls for significantly higher capacity and flexibility [1]. Aforementioned system requirements, in conjunction with technological developments such as solid state amplification and digitally transparent processors, drive the development of active antenna systems for emerging telecommunication satellite payloads. Direct Radiating Arrays (DRAs) is a favorable solution as they offer high degree of flexibility and performance.

In order to achieve the required levels of gain, a very high number of radiating elements are needed in a DRA architecture. Direct digital control of each individual element is well beyond the Digital Transparent Processor (DTP) state-of-the-art [2]. Instead, a hybrid analogue-digital beamforming architecture exploiting digitally controlled subarrays, which in turn implement analogue beamforming, provides a solution to split the system into a cascade of analog and digital beamforming [2]. Then, the number of digital controls is drastically reduced. This hybrid beamforming architecture is presented on Fig. 1.

Whilst DRAs exploiting analogue beamforming subarrays have favourable performance when the beam points at broadside, they suffer from increased grating lobes when the primary beam scans. In the literature, a solution is proposed in [3] where the subarrays are overlapped with adjacent subarrays. This solution is an efficient way to suppress some of the grating lobes. However from an implementation point of view, it requires different type of active elements across the array.

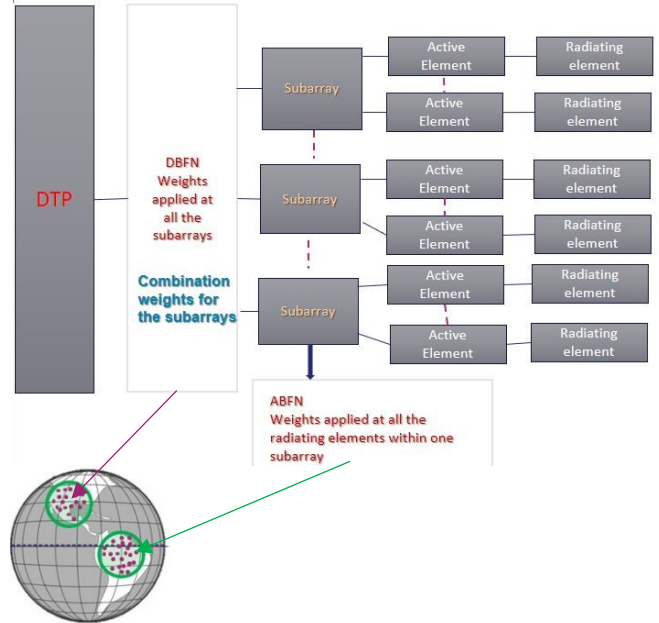


Fig. 1. Hybrid beamforming composed of a cascade of analogue and digital beamforming. ABFN influence on the regional beam in green. DBFN influence on spot beams in purple.

This contribution proposes an alternative antenna architecture that exploits overlapped subarrays. The proposed architecture relies on amplifiers that are identical along most of the array. As will be shown, the proposed architecture enables scanning to wider angles for a given drop in gain when compared to non-overlapped cases. An efficient modelling tool for the proposed architecture has been developed and applied in a comparative performance of DRAs exploiting analogue beamformed subarrays.

II. A DESCRIPTION OF OVERLAPPED ARRAYS SHIFTED BY HALF THE SIZE OF A SUBARRAY ALONG 2-D

A. Overlap methodology

The overall antenna can be thought of as the superposition of two antenna arrays, which share the same active radiating elements, as described on Fig. 2. Each antenna array consists of subarrays (tiles) in a regular periodic arrangement. The first array is identified as the one with subarrays in continuous line, while the second is defined by subarrays in dot line.

The radiation pattern of each tile, which in turn comprises a number of radiating elements, is controlled by an analogue beamforming network (ABFN). All subarrays and ABFNs are identical and produce the same radiation pattern, whose main lobe in the remaining is referred to as Regional Beam.

A digital beamforming network (DBFN) provides complex weights across the various subarrays (tiles) to form highly directive beams as described on Fig.1.

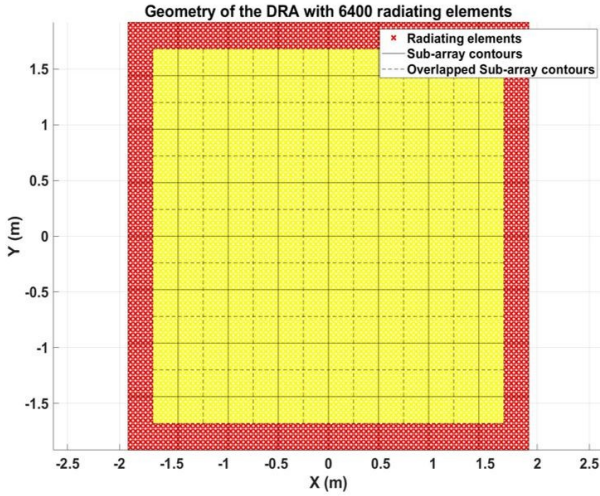


Fig. 2. Configuration for overlapping with half the size of a subarray along 2D. In red, radiating elements fed by 1 subarray. In yellow, radiating elements fed by 2 subarrays.

The two antenna arrays on Fig. 2, whose superposition leads to the proposed antenna architecture, are identical except potentially from some difference in the number of subarrays (tiles) they comprise (often the inner array has less tiles than the outer one). Moreover the two arrays are shifted with respect to each other. It is noted that in practice the two antenna arrays share the same set of radiating elements. In other words, the overall antenna can be seen as a superposition of two independent hybrid analogue digital beamforming networks that feed the same set of radiating elements.

Depending on the relative size of the subarrays/tiles, different scenarios can be considered. In this paper we assume that

- The subarrays/tiles are square with dimensions equal to the periodicity of the lattice along which they are arranged.
- The relative shift between the two arrays is equal to half of the dimensions of the subarray along both directions of the antenna plane

An efficient formulation for a generalized case that is not constrained by the above requirements has been developed and is here used to produce the radiation characteristics of the proposed antenna as well as the conventional architecture with non-overlapped subarrays.

Elements in yellow on Fig. 2 are fed by two subarrays. In red, the radiating elements are fed by one subarray. Array 1 can be defined as all the elements fed by one or two subarrays whereas Array 2 is only represented by elements in yellow. As discussed, the ABFN is the same across all the subarrays across the two arrays. Since the number of tiles is different, the DBFN weights are not the same. In practice, the DBFN contribution of Array 2 to the radiating elements is higher.

B. ABFN and DBFN weights combination

The knowledge of complex weights on the radiating elements from both arrays is mandatory to calculate the weights of the final array. Let's define $W_{ABFN} \in \mathbb{C}^{n_x \times n_y}$ the

complex ABFN weights, including amplitude and phase, where n_x and n_y are the number of elements within each subarray along x and y axis. The DBFN weights $W_{DBFN_1} \in \mathbb{C}^{N_{subx_1} \times N_{suby_1}}$ and $W_{DBFN_2} \in \mathbb{C}^{N_{subx_2} \times N_{suby_2}}$, where (N_{subx_i}, N_{suby_i}) is the number of subarrays within Array i along x and y axis, are attributed to respectively Array 1 and Array 2.

It is noted that all elements of Array 2 contribute to both Array 1 and Array 2. Consequently, in order to estimate the signal radiated from these elements, we need to add the total complex weights associated with Array 1 and 2. This step requires identifying each individual radiating element, and thus apply power normalization at element level. We introduce W_{T_1} and $W_{T_2} \in \mathbb{C}^{n_x N_{subx_1} \times n_y N_{suby_1}}$ that represent the final complex weights with which each radiating element is excited due to their contribution in Array 1 and 2 respectively. Both matrices can be described as :

$$W_{T_1} = \begin{pmatrix} W_{DBFN_{11}} W_{ABFN_{11}} & W_{DBFN_{11}} W_{ABFN_{1n_y}} & \dots & W_{DBFN_{1N_{suby_1}}} W_{ABFN_{1n_y}} \\ W_{DBFN_{11}} W_{ABFN_{n_x1}} & W_{DBFN_{11}} W_{ABFN_{n_x n_y}} & \dots & W_{DBFN_{1N_{suby_1}}} W_{ABFN_{n_x n_y}} \\ \vdots & \vdots & \ddots & \vdots \\ W_{DBFN_{11}} W_{ABFN_{11}} & W_{DBFN_{11}} W_{ABFN_{1n_y}} & \dots & W_{DBFN_{1N_{suby_1}}} W_{ABFN_{1n_y}} \\ W_{DBFN_{11}} W_{ABFN_{n_x1}} & W_{DBFN_{11}} W_{ABFN_{n_x n_y}} & \dots & W_{DBFN_{1N_{suby_1}}} W_{ABFN_{n_x n_y}} \\ \vdots & \vdots & \ddots & \vdots \\ W_{DBFN_{1N_{subx_1}}} W_{ABFN_{11}} & W_{DBFN_{1N_{subx_1}}} W_{ABFN_{1n_y}} & \dots & W_{DBFN_{1N_{subx_1} N_{suby_1}}} W_{ABFN_{1n_y}} \\ W_{DBFN_{1N_{subx_1}}} W_{ABFN_{n_x1}} & W_{DBFN_{1N_{subx_1}}} W_{ABFN_{n_x n_y}} & \dots & W_{DBFN_{1N_{subx_1} N_{suby_1}}} W_{ABFN_{n_x n_y}} \end{pmatrix} \quad (1)$$

$$W_{T_2} = \begin{pmatrix} 0_{\frac{n_x}{2} \times \frac{n_y}{2}} & 0_{\frac{n_x}{2}} & \dots & 0_{\frac{n_y}{2}} & \dots & 0_{\frac{n_x}{2} \times \frac{n_y}{2}} \\ 0_{\frac{n_x}{2}} & W_{DBFN_{211}} W_{ABFN_{n_x n_y}} & \dots & W_{DBFN_{21j}} W_{ABFN_{n_x k}} & \dots & 0_{\frac{n_x}{2}} \\ \vdots & \vdots & \ddots & \vdots & \ddots & \vdots \\ 0_{\frac{n_x}{2}} & W_{DBFN_{2i1}} W_{ABFN_{1n_y}} & \dots & W_{DBFN_{2ij}} W_{ABFN_{1k}} & \dots & 0_{\frac{n_x}{2}} \\ 0_{\frac{n_x}{2}} & W_{DBFN_{2i1}} W_{ABFN_{n_x n_y}} & \dots & W_{DBFN_{2ij}} W_{ABFN_{1k}} & \dots & 0_{\frac{n_x}{2}} \\ \vdots & \vdots & \ddots & \vdots & \ddots & \vdots \\ 0_{\frac{n_x}{2}} & W_{DBFN_{2N_{subx_2}1}} W_{ABFN_{1n_y}} & \dots & W_{DBFN_{2N_{subx_2}j}} W_{ABFN_{1k}} & \dots & 0_{\frac{n_x}{2}} \\ 0_{\frac{n_x}{2} \times \frac{n_y}{2}} & 0_{\frac{n_x}{2}} & \dots & 0_{\frac{n_y}{2}} & \dots & 0_{\frac{n_x}{2} \times \frac{n_y}{2}} \end{pmatrix} \quad (2)$$

Finally, the matrix W_T that describes the overall complex amplitudes with which each element is radiating can now be calculated :

$$W_T = W_{T_1} + W_{T_2} \quad (3)$$

Next the power normalization is performed for the complex weights in order to ensure that the power radiated from each element does not exceed the output power of the associated amplifier. Then, W_T must be normalized to W_{T_n} so that the total power cannot exceed unity:

$$W_{T_n} = \frac{W_T}{\|W_T\|} \quad (4)$$

Once we have identified W_{T_n} the radiation pattern of the entire array can be obtained by:

$$A_{tot}(u, v) = E(u, v) \sum_{l,k}^{n_x N_{sub1_x}, n_y N_{sub1_y}} W_{T_{nlk}} e^{j \frac{2\pi}{\lambda} (x_{RE_l} u + y_{RE_k} v)} \quad (5)$$

where (x_{RE_l}, y_{RE_k}) are the coordinates of the (l, k) radiating element. It is noted that the analog and digital beamforming are performed jointly to compute A_{tot} .

III. BENCHMARK OF THE OVERLAPPING STRATEGY

A. Radiation pattern

Since the expression of A_{tot} has been defined, the expression with the total combined weights is used to calculate the radiation pattern. A study has been undertaken to find the optimal taper in terms of gain and scanning performance (details not shown for brevity). The results presented in this paper are then computed with a 3dB taper in terms of power [2]. The 3dB taper at ABFN level is an efficient solution to enlarge the scanning area, by broadening the subarray pattern, i.e the size of the area beam is increased. However, the gain is also decreased as a consequence of this broadening. The 3 dB taper is then the best compromise between being able to scan further and reaching a high gain within a regional area.

The scanning range is introduced as a parameter to benchmark the different architectures. This value corresponds to the angular range for which the gain scan loss is less than 3dB. In this contribution, the spot beams are scanned within the main regional beam area, i.e at DBFN level. For the study, the regional beam is not steered and is thus situated at nadir. The scanning range is targeted as high as possible, i.e the scan loss is lowered as much as possible.

The architectures we consider are shown on Fig. 2. The initial architecture is defined as the non-overlapped one, and involves 8×8 subarrays of 10×10 radiating elements (subarrays in continuous line only). The overlapped array is computed with $8 \times 8 + 7 \times 7$ subarrays of 10×10 shared radiating elements (both subarrays in continuous and dot lines). The overlapped array and the non-overlapped one have both 6400 radiating elements and are computed at 20 GHz. The addition of an overlapping array thus implies that the number of digital controls (DCs) is different across non-overlapped and the overlapped case; the non-overlapped array has 64 DCs against 113 DCs for the overlapped array.

A cut of the radiation pattern along A-axis is shown on Fig. 3 for a scanned beam. A is the $\phi = 0^\circ$ axis projected on Earth, where ϕ is the elevation angle. B-axis used later on Fig. 4. is the projection on Earth of $\phi = 90^\circ$ axis. This cut enables to observe the gain and grating lobe changes brought by the overlapping methodology. The spot beams are scanned at 0.8° along A-axis.

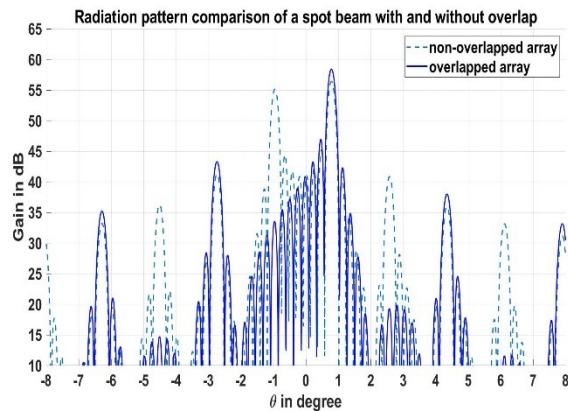


Fig. 3. Simulated radiation pattern cuts along the axis. Scan along A at 0.8° . In dot lines, non-overlapped array, in continuous line, overlapped array.

In terms of gain, 58.42 dBi can be shown for the overlapped array against 56.43 dBi for the basic non-overlapped architecture. Thus, a difference of 1.99 dBi is

observed between the two cases. The possibility to scan further with reduced gain degradation along the A-axis is then a benefit of the overlapped architecture.

The same 1.99 dBi increase is shown at even grating lobes for the overlapped array. On the contrary, the odd grating lobes are totally mitigated. The first order grating lobes which are the closest to the main beam are suppressed. A very high gain is then maintained at the main beam. These first order grating lobes are the limit of the non-overlapped architecture. It can be observed that the grating lobe on the left of the main beam at -1.2° is at 55.16 dBi which is less than 2 dB difference with the main beam for the non-overlapped case. Interference are thus created by this grating lobe.

So far, only a cut has been studied. The gain increase and grating lobe mitigation have been checked along only one direction. However, the grating lobe lattice can be observed as well. From a theoretical point of view, adding a 7×7 rectangular feed plane shifted by half the size of a subarray can be seen as a transformation of the initial rectangular subarray lattice into a triangular one. Fig. 4. thus shows the lattice while scanning at 0.5° along the diagonal.

A triangular grating lobe lattice is generated in the overlapped case. By comparing the non-overlapped lattice with the overlapped one, it is noticed that the triangular lattice is generated thanks to the mitigation of odd $(p + q)$ grating lobes, where p is the index of the grating lobe along B axis and q the index of the grating lobe along A-axis. Then, along the axis, the first order grating lobes are totally mitigated. However, the diagonal first-order grating lobes are still present in the overlapped case. Along the diagonals an improvement of the gain while scanning is thus limited. Along the other planes, the impact of this non-mitigated grating lobe is limited and its level is still reduced.

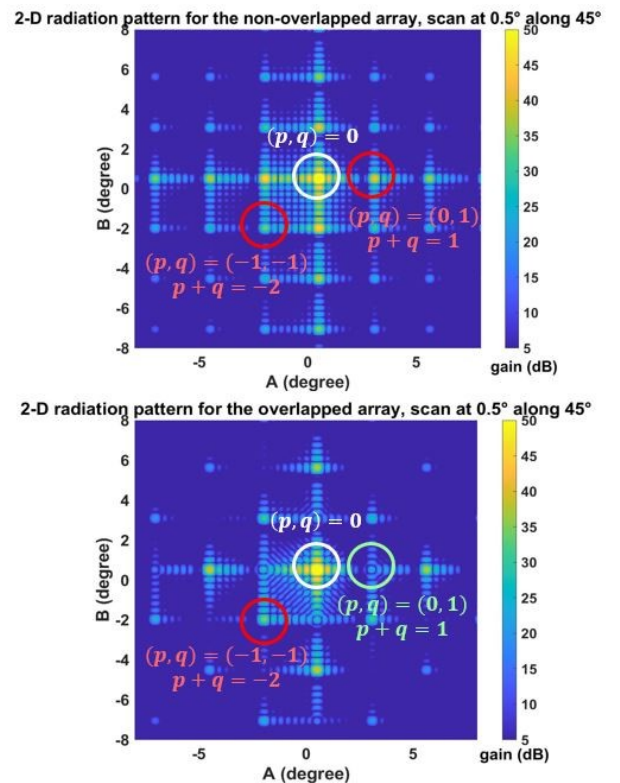


Fig. 4. View from the top of the 3D radiation pattern. On the top, the non-overlapped case. On the bottom, the overlapped case

B. Amplitude and phase distribution

The increase of the gain can be explained by the amplitude of the elements across the entire array. Fig. 5 shows the amplitude distribution while scanning at 0.8° along A-axis for the overlapped case when a 3 dB taper is applied. In theory, the radiating aperture and therefore the gain is optimal if the power, or amplitude, is the most uniform as possible.

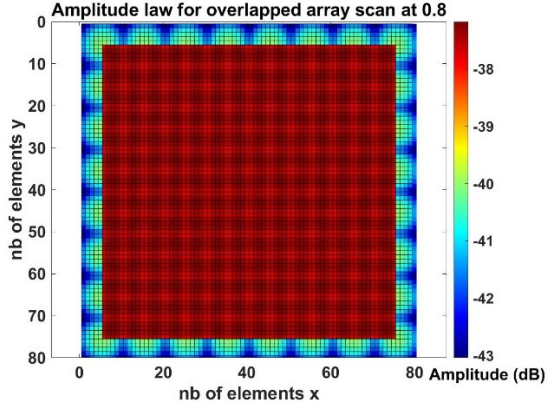


Fig. 5. Amplitude distribution element per element for the overlapped array while scanning at 0.8° along A-axis.

The amplitude is higher and close to a uniform distribution at the center of the architecture where Array 1 and Array 2 are overlapped. On the contrary, the amplitude is lower at the edge. This can be explained by the number of subarrays to which each element contributes. At the edge, only one feed is used per radiating element. Then, half of the power is provided by Array 1 before normalization. The other half of the power before normalization is brought by Array 2. The power is then almost doubled at the center compared to the edge.

It is noted that when the beam is scanned, the power at the edge is increased, and the power at the center is decreased. This is due to the phase opposition between Array 1 and Array 2. The phase is thus not summed in coherence. At nadir, there is no need for phase compensation. While scanning, the phase opposition is compensated by the power normalization so that power loss is prevented.

The grating lobe mitigation information are linked to the phase of the radiating elements. The phase study is given on Fig. 6. when the beam is scanned at 0.8° along A-axis. A characteristic of the phase distribution that can be observed is its step variations. The presence of these steps is associated with grating lobes. The objective is thus to smoothen the phase so that the grating lobes are mitigated. Smaller steps are generated with the overlapping strategy than without overlap at the center of the architecture, i.e. within the overlapping area. A smoothing of the phase is done thanks to this smaller variations. The grating lobe mitigation is confirmed by the phase study.

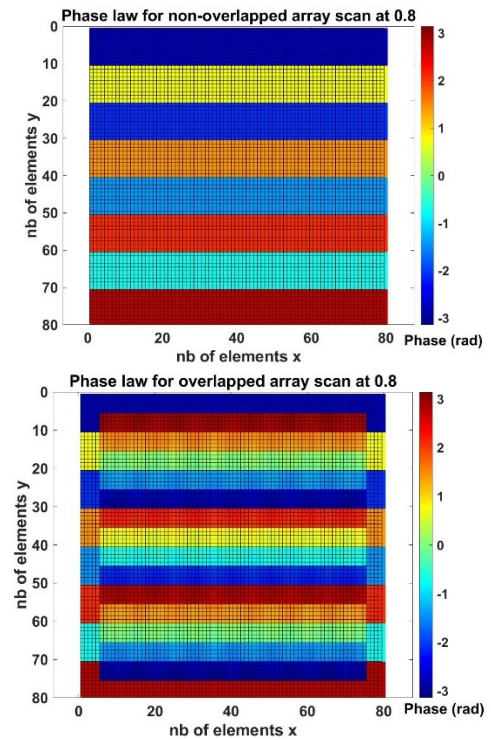


Fig. 6. Phase element per element for the overlapped array (bottom) and non-overlapped array (top) while scanning at 0.8° along A-axis.

IV. PERFORMANCE EVALUATION THANKS TO A COMPARISON WITH A CLOSE NUMBER OF DIGITAL CONTROLS

The number of digital controls (DCs) is an influencing factor for the scanning range improvement. So far, the benchmark of the overlapped methodology has been shown with 113 DCs. The idea is now to evaluate the performance of the overlapping methodology, called overlapped array (OA). A comparison is made with another strategy with the closest number of digital controls. A new architecture is thus needed to be defined for the non-overlapped case (NO) so that the interest of the overlapping strategy is shown. The closest number of DCs that can be generated with a similar architecture, i.e. same rectangular shape of subarrays and 6400 radiating elements, is 100 DC. A closest number of DCs can be found with 10×11 subarrays of 8×8 elements, but the radiating aperture would be different and the benchmark would be even more biased.

All architectures are summed up in Table. 1.

TABLE I. ARCHITECTURE DEFINITIONS

Architecture name	Parameters		
	Number of subarrays	Number of radiating elements within each subarray	Number of DCs
NO	10×10	8×8	100
OA	8×8	10×10	113

The scanning range for which the gain loss is less than 3dB is introduced as a parameter to benchmark different architectures. A same reference gain is needed to compare architectures with very different gain at nadir. It is known that the maximal radiating aperture is reached for the most uniform electromagnetic field [4]. This case thus corresponds

to the NO case with a uniform tapering at nadir. The maximum gain is 59.15 dBi. From this maximum gain, for each architecture, the main beam is scanned along one direction from nadir, and is offset with a 0.01° step until scan losses of 3dB are reached. This scan losses are presented on Fig. 7. where cuts along 0° and along 45° azimuth directions are shown. For all architectures, the tapering optimization has been studied beforehand, such that the trade-off between the scanning range and the gain is optimized.

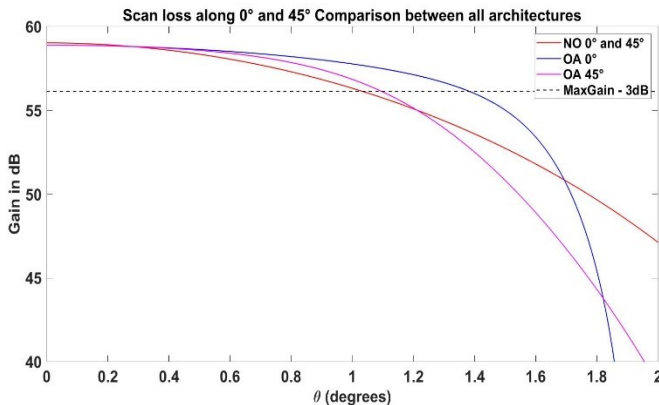


Fig. 7. Scanning range for which the gain loss is less than 3dB . Comparison for a close number of DC for all methodologies with optimized tapers. Cuts along 0° and 45° azimuth directions.

A same scanning range of 1.03° along 0° and 45° can be observed for the NO case. On the contrary, drastically different scanning range are performed along 0° and 45° directions for the OA architecture. The maximum elevation that can be reached with at least the required threshold is 1.11° along the diagonal and 1.40° along 0° . Along the principal axis, a 35.9% improvement is shown for OA compared to NO. Along the diagonal, the scanning range is increased by 7.8% thanks to the overlap.

These results can all be explained by the grating lobe lattice. For the NO case, the subarrays are smaller and thus the main regional beam is broader. The grating lobes are initially situated further to the main beam than the OA architecture for which the subarrays are larger. Along the axis, the first order grating lobes are mitigated thanks to the overlap. The first-order grating lobes generated with the NO case are thus still closer to the main beam compared to the OA architecture.

On the contrary, diagonal grating lobes are closer to the main beam for the OA case because of smaller generated subarrays for the NO architecture. However, the diagonal scanning range performance are better for the OA methodology thanks to the mitigation of grating lobes along the axes. Only one non-negligible grating lobe is interfering with the main beam. This diagonal scanning range difference is also explained by the 13 additional DCs.

A need for a study along all the azimuth directions is motivated by completely different improvements along the 45° and the 0° axes. The same process is performed from 0 to 360° with a 1° step. A scanning range surface is now presented along 2-D on Fig. 8.

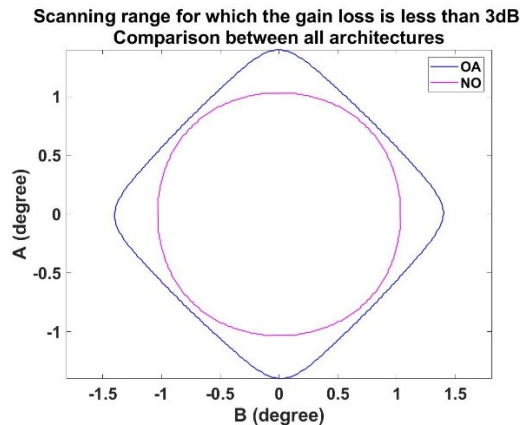


Fig. 8. Scanning range for which the gain loss is less than 3dB . Comparison for a close number of DC for all methodologies with optimized tapers along all the azimuth directions.

A square-shaped scanning range is generated for the OA methodology while a circular scan loss limit is noticed without overlap. A symmetry in the scan loss is observed and thus the minimum and best scanning ranges for the OA architecture are repeated respectively along all the diagonals and all the principal axes. This leads to a surface improvement of 47.9% for the OA compared to the NO, which is a significant increase considering a difference of 13 DCs.

V. CONCLUSION

A new direct radiating array architecture has been proposed that improves the scanning range compared to an hybrid beamforming solution. The proposed architecture exploits the overlap of two arrays and leads to the creation of a triangular lattice with square subarrays. Several tapers can be found that enable easy amplifier solutions. It has better performance than the non-overlapped solution with a close number of digital controls. The architecture is easy to set in practice in terms of electronic since the front-ends for most of the radiating elements are identical. The complete mitigation of odd grating lobes is brand new compared to other overlapping strategies and also of interest from a system point of view since it enables to process less interference. The side lobes are not significantly increased while scanning and is also of interest for future resource allocation and system performance.

ACKNOWLEDGMENT

This work has been supported by the European Space Agency under contract No. 4000135641/21/NL/GLC/my

REFERENCES

- [1] Ricardo de Gaudenzi : "Challenges in Future Satellite Communications", IEEE Communication Theory Workshop, 15th May 2018
- [2] Vidal, Florian, et al. "Joint precoding and resource allocation strategies applied to a large direct radiating array for GEO telecom satellite applications." *2021 15th European Conference on Antennas and Propagation (EuCAP)*. IEEE, 2021.
- [3] Tugend, Vincent, and Andrew Thain. "Hybrid beamforming with reduced grating lobes for satellite applications." (2018): 236-5
- [4] Robert J. Mailloux : "Phased Array Antenna Handbook" second edition, Artech House antennas and propagation library, 2005